Supporting Information for

Ultra-thin N-doped-graphene encapsulated Ni nanoparticles coupled with MoO_2 nanosheets for highly efficient water splitting at large-current-density

Guangfu Qian [†a], Guangtao Yu [†b,c], Jiajia Lu[a], Lin Luo[a], Ting Wang[c], Chenghui Zhang[c], Ruiqi Ku[c], Shibin Yin[*a], Wei Chen[*b,c], Shichun Mu[*d]

[a] College of Chemistry and Chemical Engineering, State Key Laboratory of Processing for Non-Ferrous Metal and Featured Materials, Guangxi University, Nanning 530004, China

[b] College of Chemistry and Materials Science, Fujian Normal University, Fuzhou 350007, China

[c] Laboratory of Theoretical and Computational Chemistry, Institute of Theoretical Chemistry, Jilin University, Changchun 130023, China

[d] State Key Laboratory of Advanced Technology for Materials Synthesis and Processing, Wuhan University of Technology, Wuhan 430070, China

[†] These authors contributed equally to this work.

[*] Corresponding authors email addresses: yinshibin@gxu.edu.cn (S. Yin); w_chen@jlu.edu.cn (W. Chen); msc@whut.edu.cn (S. Mu).

1. Experimental section

Theoretical models and free-energy computations on hydrogen evolution reaction.

To explore the catalytic activity and mechanism, we constructed the correlative theoretical model by employing the N-doped graphene (NC) covering the Ni(111) surface (denoted by Ni(111)@NC, **Fig. S17**), considering that experimentally covering the ultrathin N-doped carbon layer over the Ni nanoparticle can significantly enhance the HER activity for the hybrid nano-architectures. Specifically, the Ni(111) surface was modeled by the slab with six atomic layers (**Fig. S17**). Then, the N-doped graphene was employed to simulate the ultra-thin N-doped carbon layer to cover the Ni(111) surface. The 3×3 supercells were uniformly used for the Ni(111) and NC subunits in the Ni(111)@NC model (**Fig. S17**), where the lattice mismatch between them was almost negligible (within 2%).

When covering the NC layer on the Ni(111) surface, three configurations are considered: (I) N atom and some C atoms of the NC layer in the supercell were located over the top site of Ni atom, while the remaining C atoms were located over the hollow site of Ni(111) (configuration-I); (II) Some C atoms of the NC layer in the supercell were located over the top site of Ni atom, while the remaining C atoms as well as N atom were located over the hollow site of Ni(111) (configuration-II); (III) All the N/C atoms were located over the Ni-Ni-Ni hollow site on Ni(111) (configuration-III), as illustrated in **Fig. S17**.

Our computed results reveal that the configuration-I was lowest in energy among the three configurations, indicating the highest structural stability. Therefore, we choose the configuration-I as the structural model to investigate the HER activity of hybrid system, which was directly denoted as Ni(111)@NC in this work for convenience. For the Ni(111)@NC model, the above three atomic layers (NC layer and two Ni-atomic-layers) were fully relaxed, while the remaining four Ni-atomic-layers were frozen during the computational process. Moreover, for comparison purpose, the sole Ni(111) and NC were also considered.

Based on the above structural models, we theoretically evaluated the HER catalytic activities for the correlative systems by computing the adsorption free energy of H* (ΔG_{H^*}). The ΔG_{H^*} values are calculated by the formula $\Delta G_{H^*} = \Delta E_{H^*} + \Delta ZPE - T\Delta S$, in which ΔE_{H^*}, ΔZPE and ΔS were the binding energy, zero point energy change and entropy change of H* adsorption, respectively. Among them, ΔE_{H^*} was computed by using the formula $\Delta E_{H^*} = E_{slab-H} - E_{slab} - 1/2\ E_{H2}$, where E_{slab-H} was the total energy of the slab model with the adsorbed H*, E_{slab} was the total energy of the pristine slab, and E_{H2} was the total energy of single hydrogen molecule, respectively. Moreover, the $T\Delta S$ and ΔZPE can be obtained by following the scheme proposed by Norskov *et al*.[1] Specifically, ΔS can be obtained by the equation $\Delta S = S_{H^*} - 1/2 S_{H2} \approx -1/2\ S_{H2}$, in view of the negligible vibrational entropy of H*. Thus, the $T\Delta S$ value should be –0.205 eV,

since TS(H_2) was known to be 0.41 eV for H_2 at 300 K and 1.0 atm. Additionally, the equation $\Delta ZPE = ZPE(H^*) - 1/2ZPE(H_2)$ was used to estimate ΔZPE for H*. It was worth mentioning that our computed $ZPE(H_2)$ value was about 0.298 eV, which was closed to the one reported by Norskov *et al*.[1] Finally, the computed ΔG_{H^*} results and the correlative detailed discussions were presented in the main text.

2. Supplementary figures

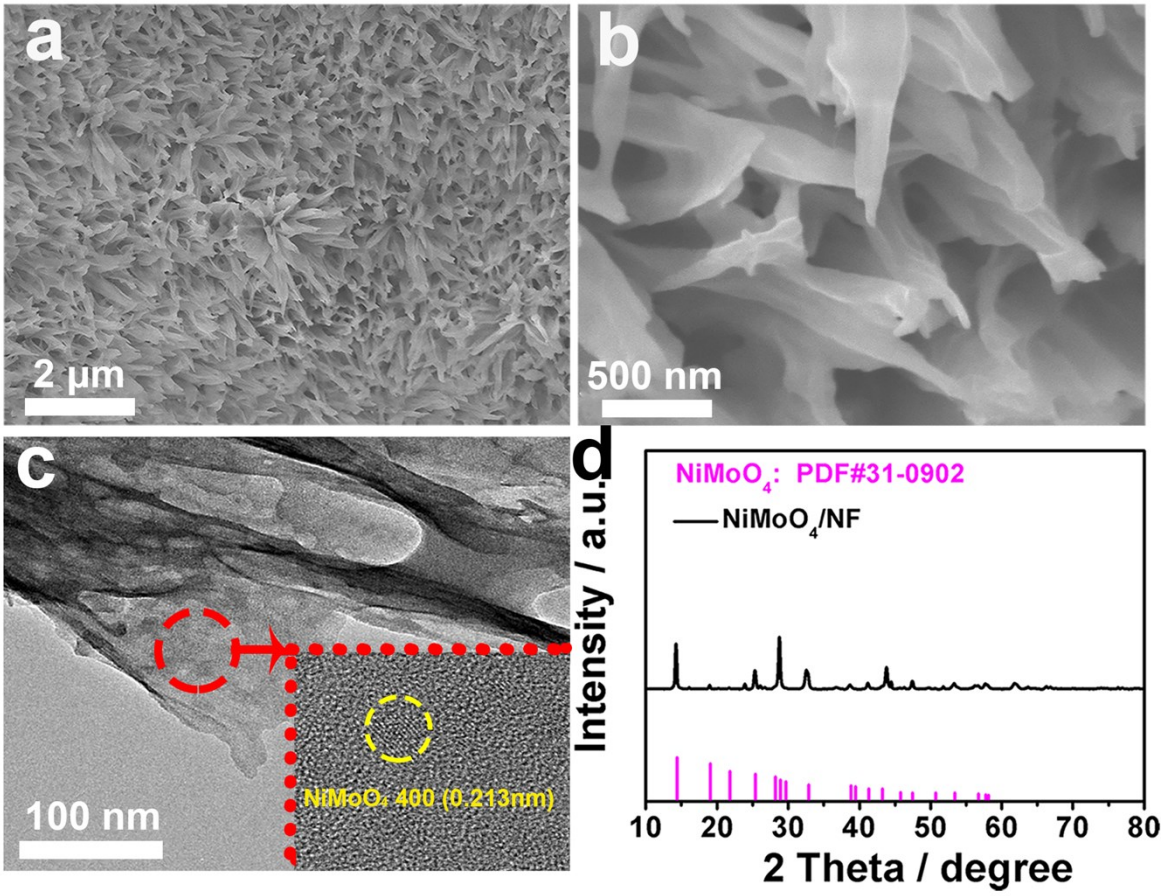

Fig. S1. (a-d) SEM, TEM, and XRD images of $NiMoO_4$/NF.

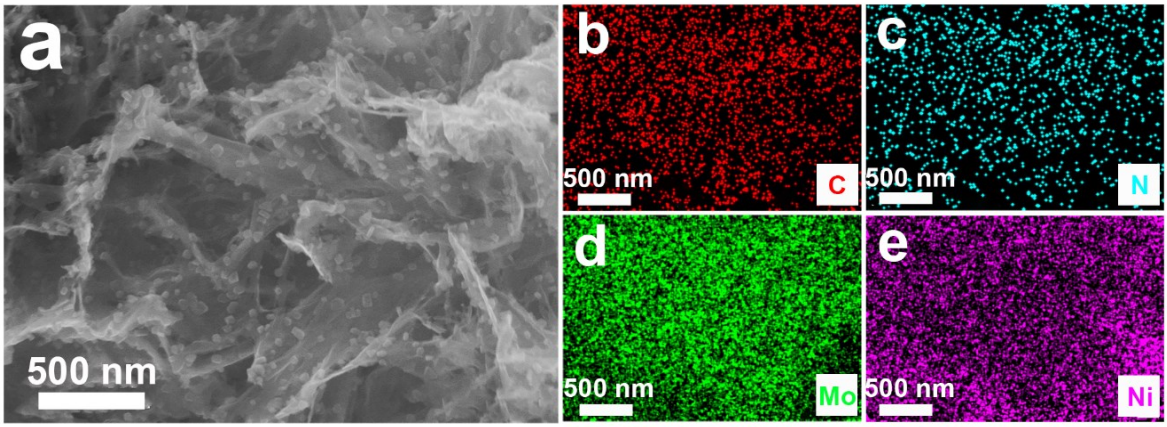

Fig. S2. SEM images of Ni@C-MoO_2/NF.

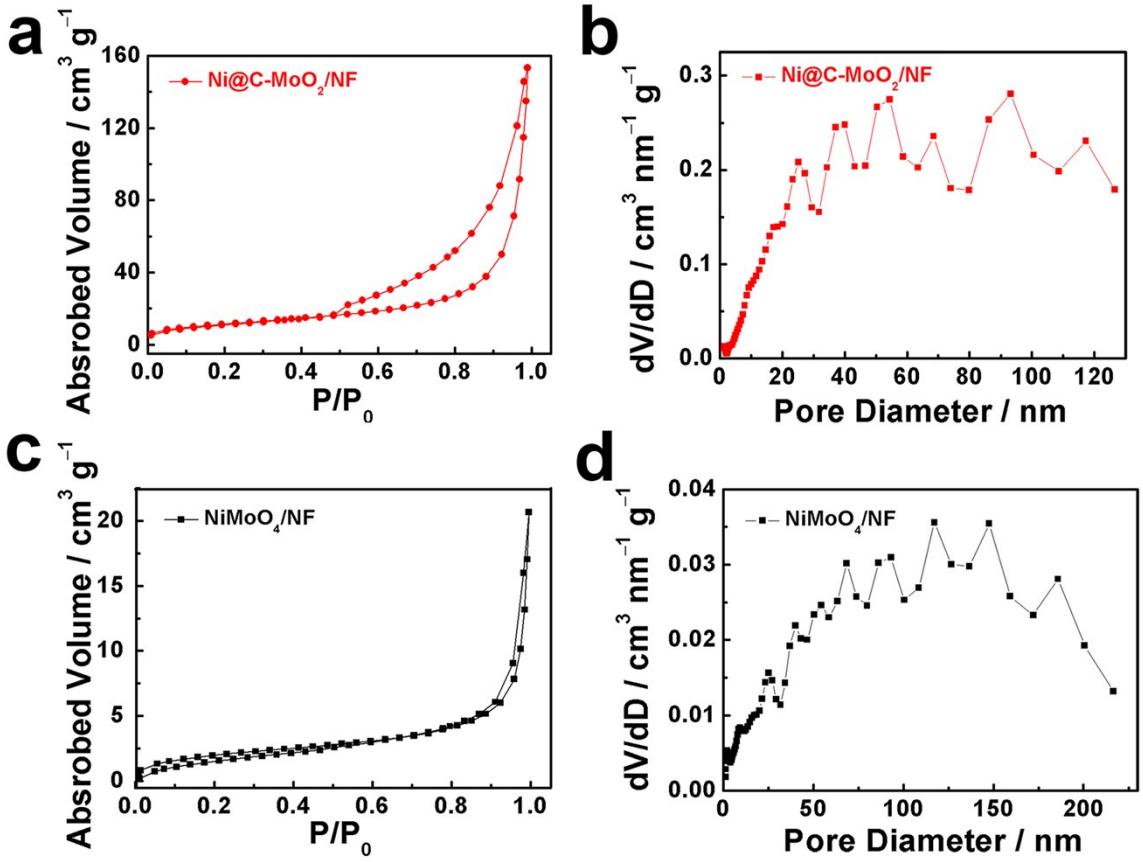

Fig. S3. (a, c) N_2 adsorption-desorption isotherms and (b, d) the corresponding pore size distributions of Ni@C-MoO_2/NF and $NiMoO_4$/NF.

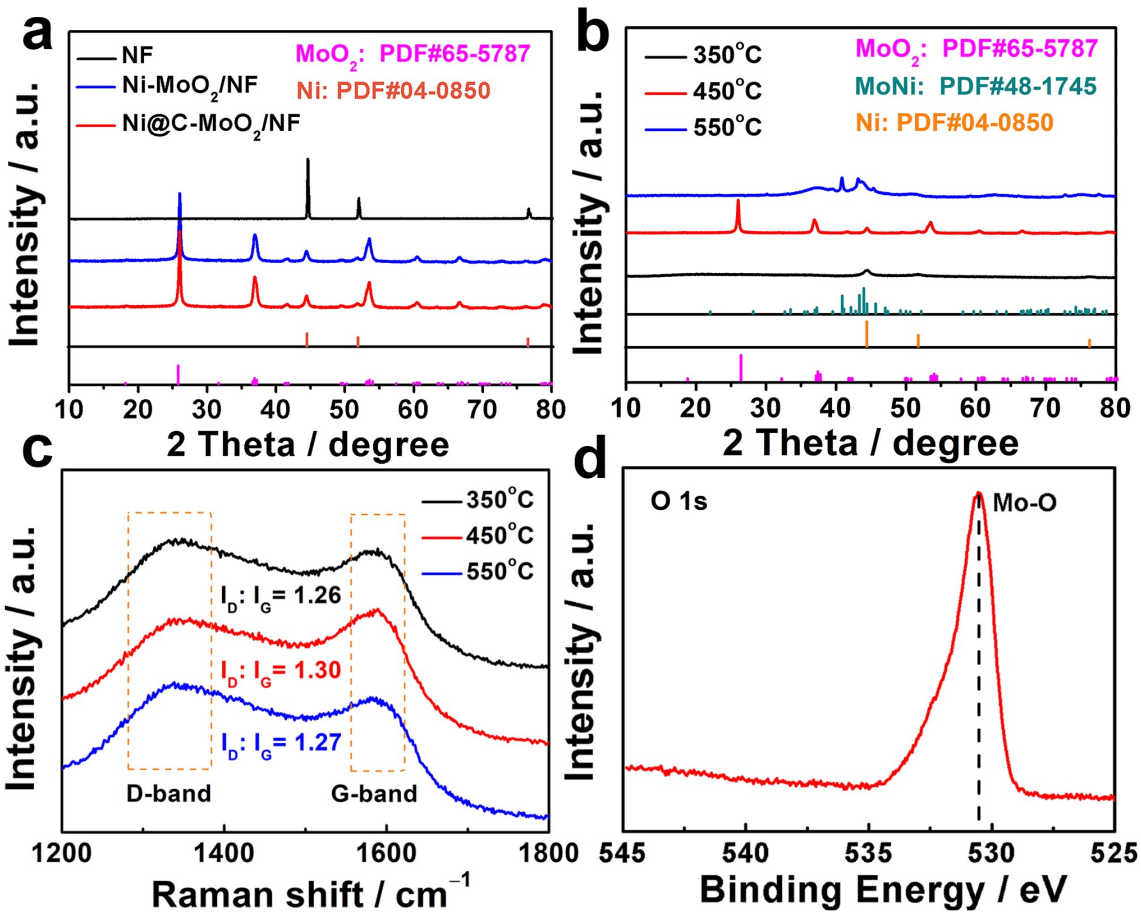

Fig. S4. (a) XRD curves of Ni@C-MoO_2/NF, Ni-MoO_2/NF, and NF; (b, c) XRD and Raman curves of Ni@C-MoO_2/NF annealed at different temperatures; (d) O 1s of Ni@C-MoO_2/NF.

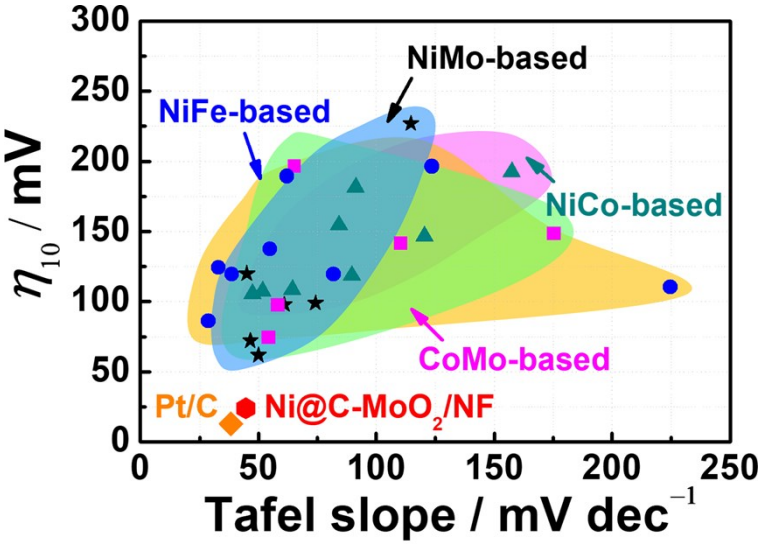

Fig. S5. Activity comparisons of references for HER. The overpotential (η_{10}) and voltage at a current density of –10 mA cm^{-2}.

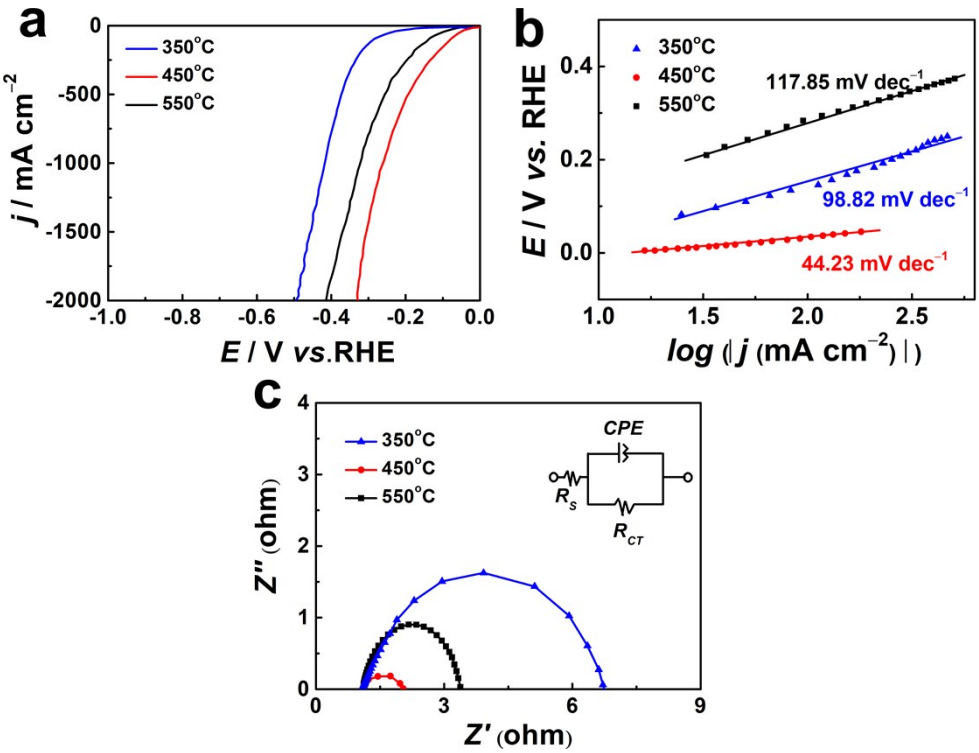

Fig. S6. (a) LSV curves of HER for Ni@C-MoO_2/NF at different temperatures; (b) Corresponding Tafel slopes; (c) Corresponding Nyquist plots tested at −0.20 V for HER with a frequency from 100 kHz to 100 mHz in 1.0 M KOH; Inset is the equivalent circuit model.

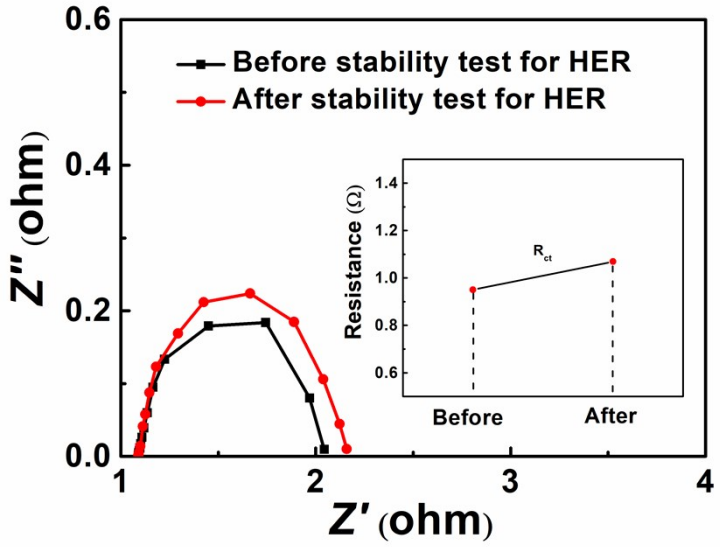

Fig. S7. R_{ct} of Ni@C-MoO_2/NF before and after hydrogen evolution stability tests by chronopotentiometry method.

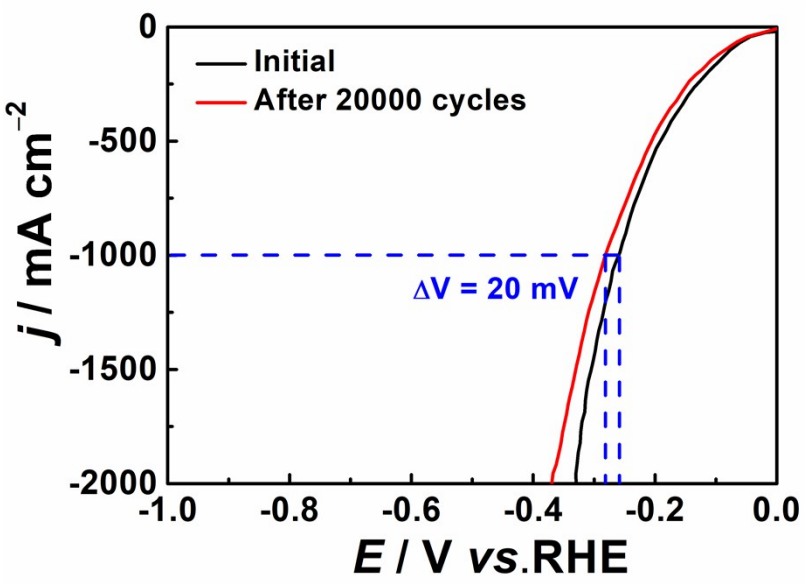

Fig. S8. LSV curves of Ni@C-MoO_2/NF for HER initially and after 20,000 CV cycles, between −0.6 V and 0 V.

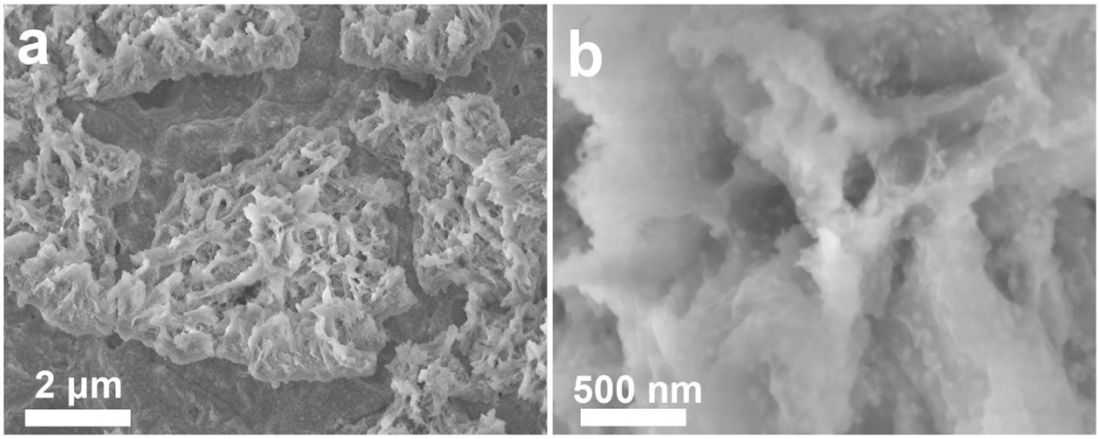

Fig. S9. SEM images of Ni@C-MoO_2/NF after hydrogen evolution stability test.

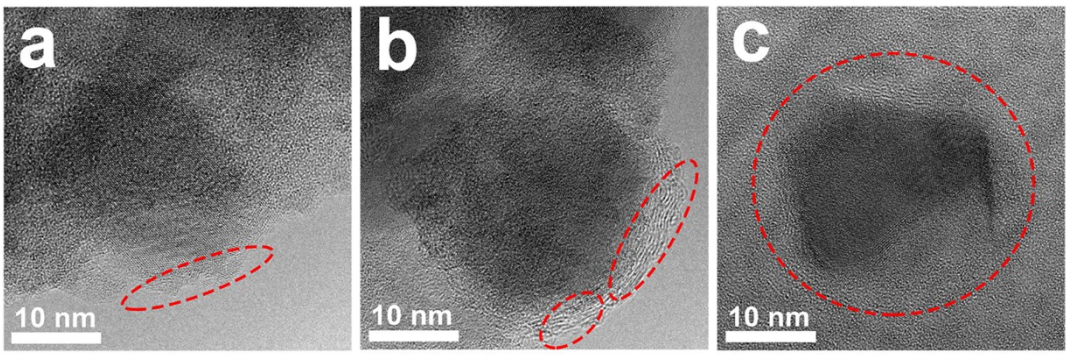

Fig. S10. HRTEM images of Ni@C-MoO_2/NF after hydrogen evolution stability test.

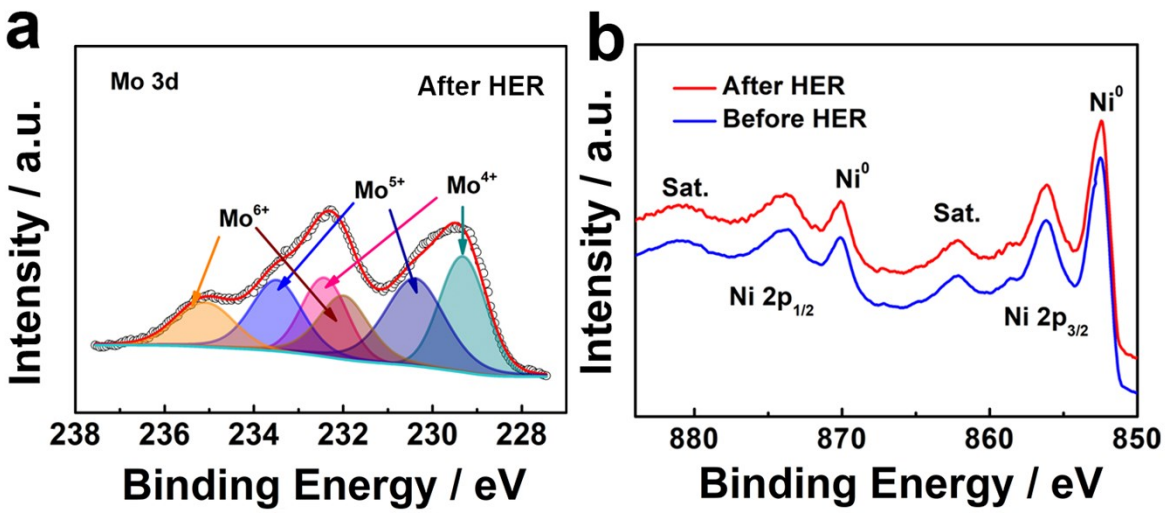

Fig. S11. XPS images of Ni@C-MoO_2/NF for Ni 2p and Mo 3d after hydrogen evolution stability test.

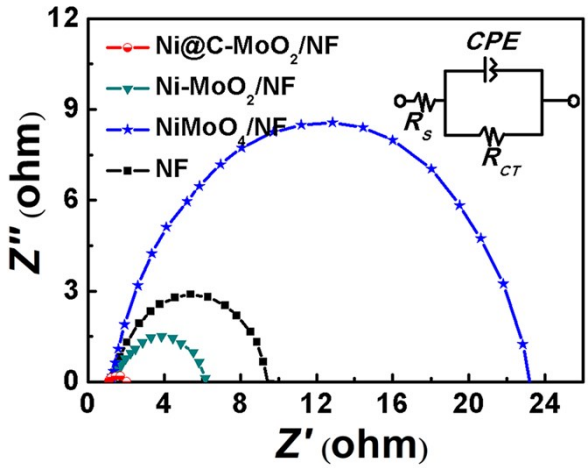

Fig. S12. Nyquist plots tested at −0.20 V for HER with a frequency from 100 kHz to 100 mHz in 1.0 M KOH; Inset is the equivalent circuit model.

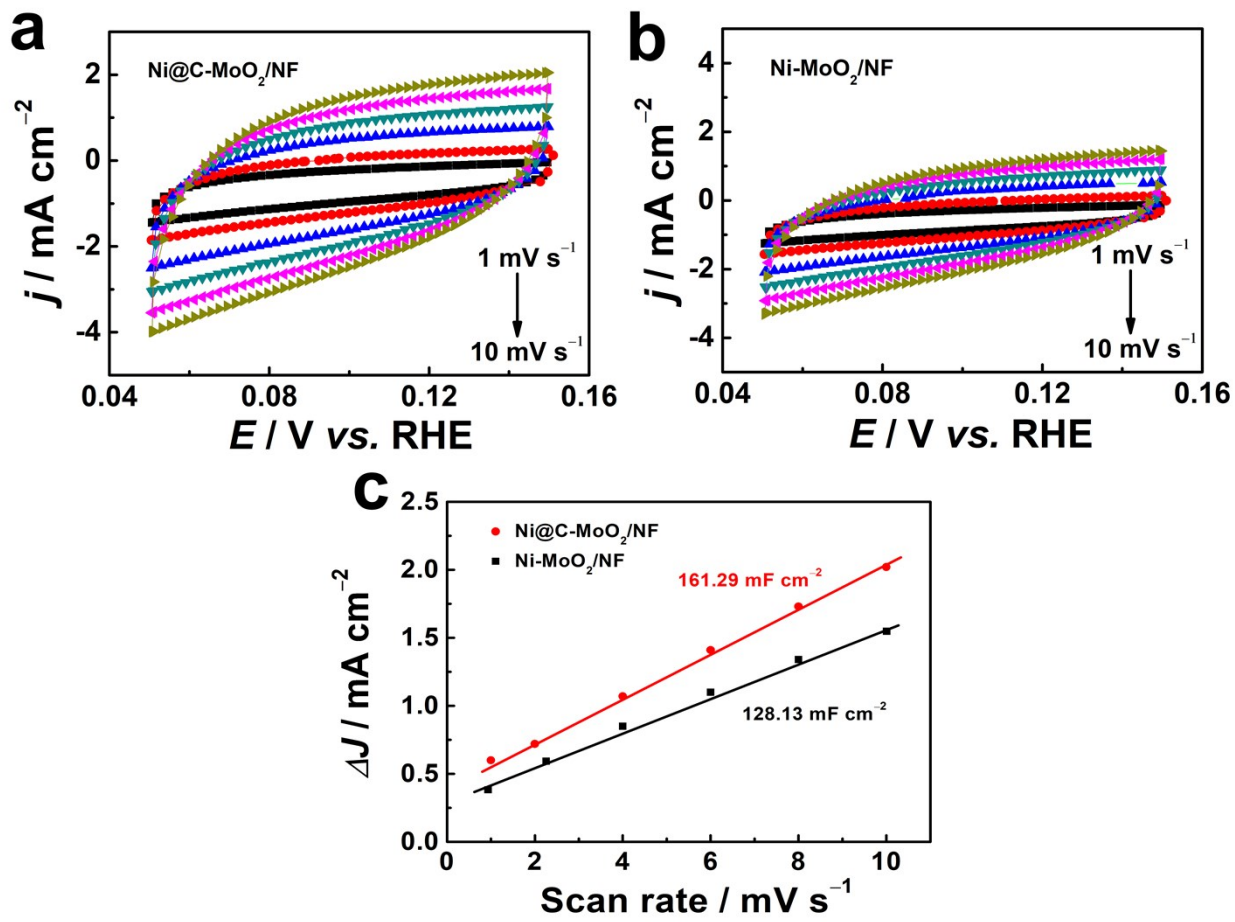

Fig. S13. (a, b) Typical CVs of Ni@C-MoO_2/NF and Ni-MoO_2/NF at scan rates ranging from 1 to 10 mV s^{-1}, the scanning potential range is from 0.05 V to 0.15 V; (c) Estimation of C_{dl} by plotting the capacitive current density against the scan rate to fit a linear regression of Ni@C-MoO_2/NF and Ni-MoO_2/NF.

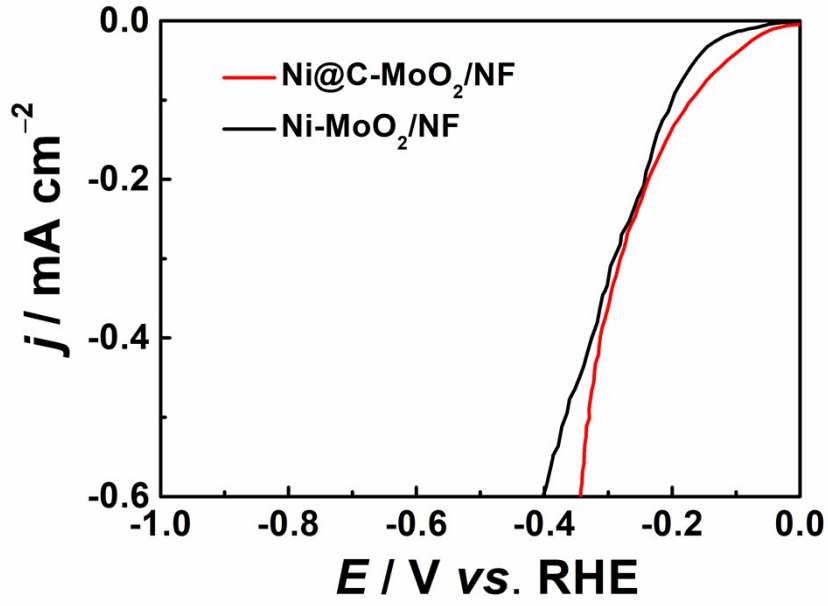

Fig. S14. HER activitiy (current density) of the samples normalized by their ECSAs.

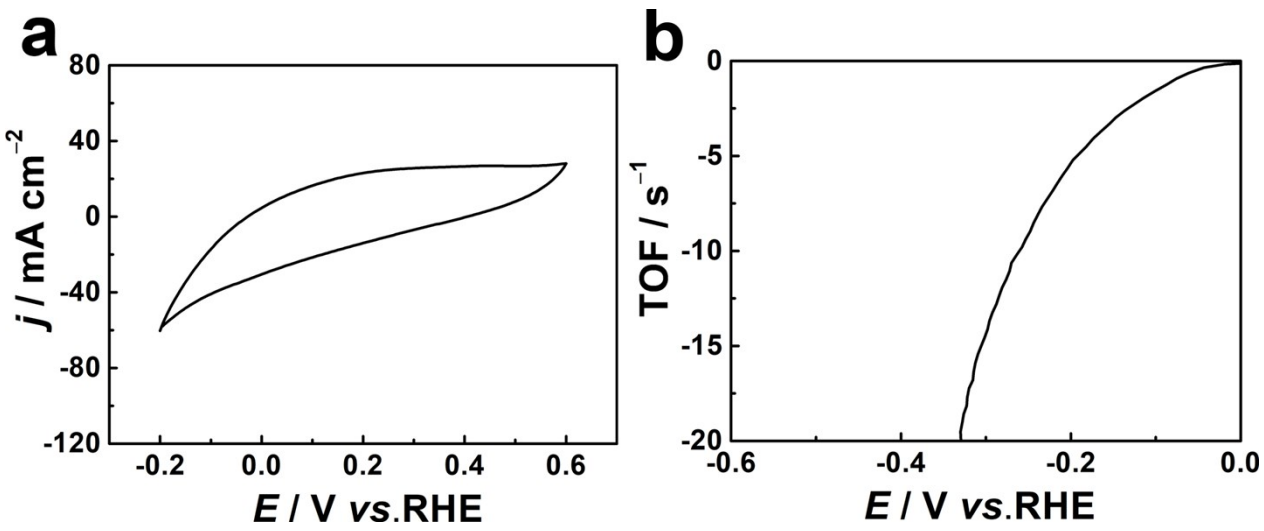

Fig. S15. (a) CV curve of Ni@C-MoO_2/NF in 1.0 M PBS (pH = 6.87) with a scan rate of 50 mV s^{-1}; (b) The calculated TOFs curve of Ni@C-MoO_2/NF for HER.

We use the CV method to study the TOFs of Ni@C-MoO_2/NF for HER.[2] As shown in Fig. S15a, the Ni@C-MoO_2/NF is tested in 1.0 M phosphate buffer solution (PBS, pH = 6.87) and the region is −0.2 to 0.6 V vs. RHE. The total number of active atoms should be proportional to the potential region range. In Fig. S15b, the polarization curve is normalized by the active sites and expressed in terms of TOFs, and the TOFs at −100 mV are 1.6 s^{-1} in alkaline media, which is higher than previous reports.[3-5] The high TOFs value of HER could be ascribed to the ultra-thin N-doped-graphene encapsulated Ni structure, which can increase the intrinsic activity of active sites to improve the catalytic activity for HER.[6-8]

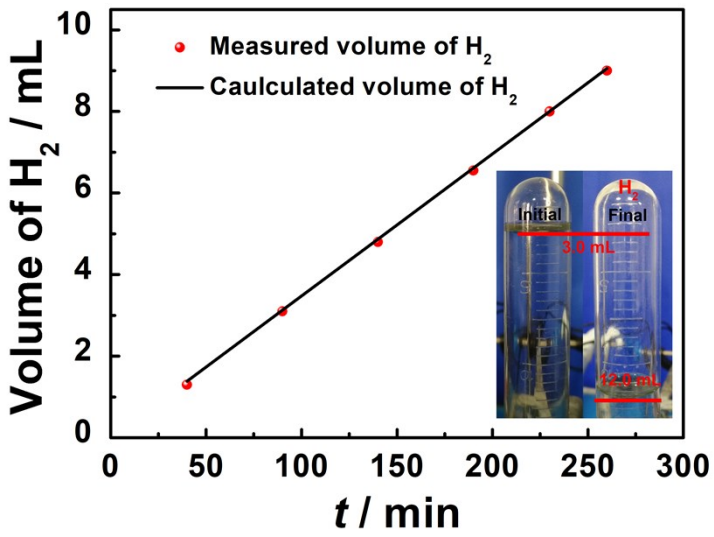

Fig. S16. Amount of hydrogen theoretically calculated and experimentally measured at the current of 5.0 mA versus time for Ni@C-MoO_2/NF in 1.0 M KOH aqueous solution. Inset: the photo indicates that the volume of hydrogen after 260 minutes is 9.0 ml.

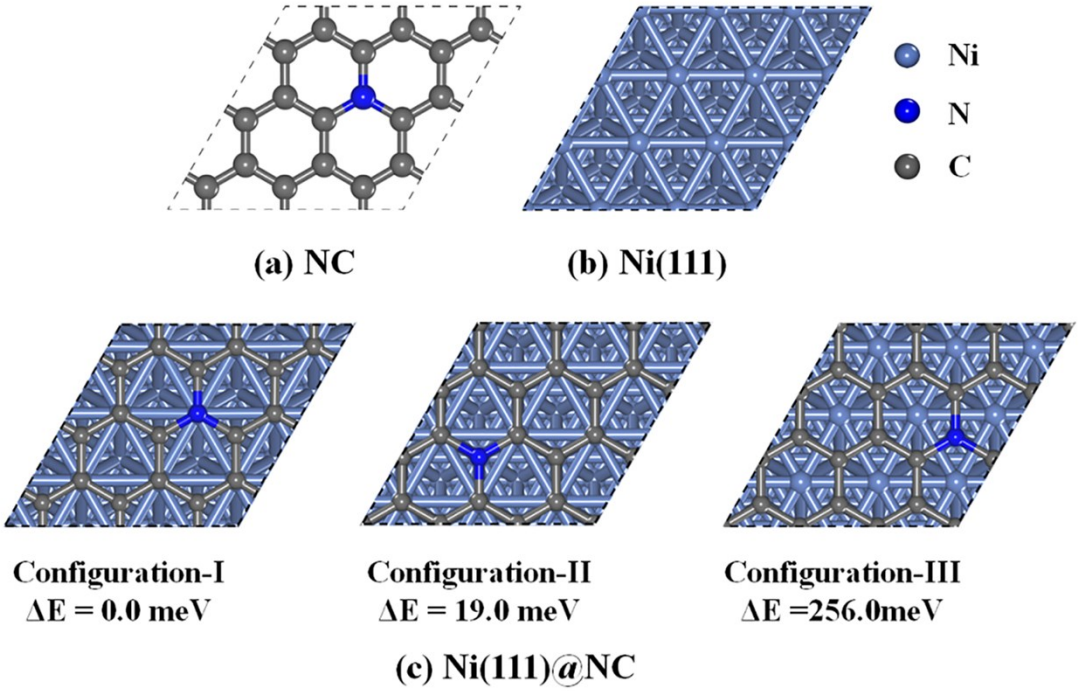

Fig. S17. The theoretical models used in DFT calculations: (a) NC, (b) Ni(111), (c) Ni(111)@NC (I~III).

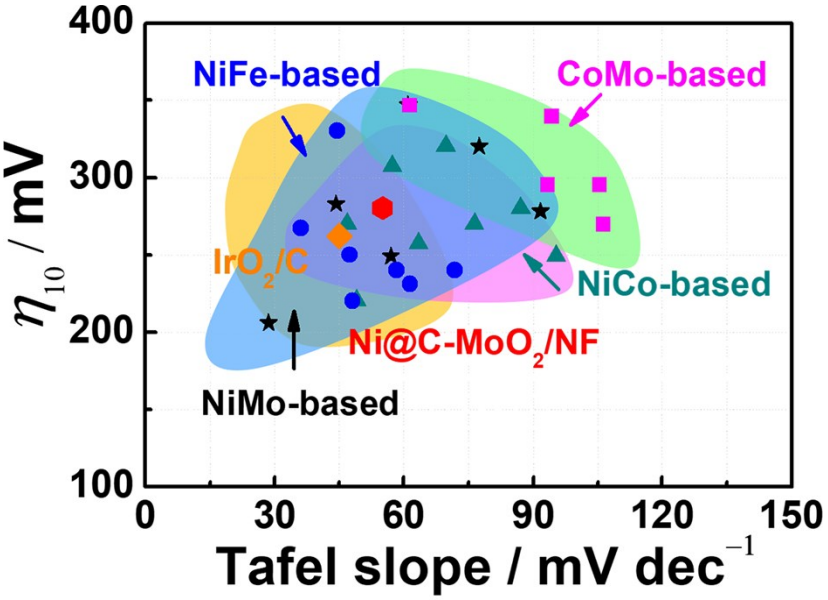

Fig. S18. Activity comparisons of references for OER. The overpotential (η_{10}) and voltage at a current density of 10 mA cm^{-2}.

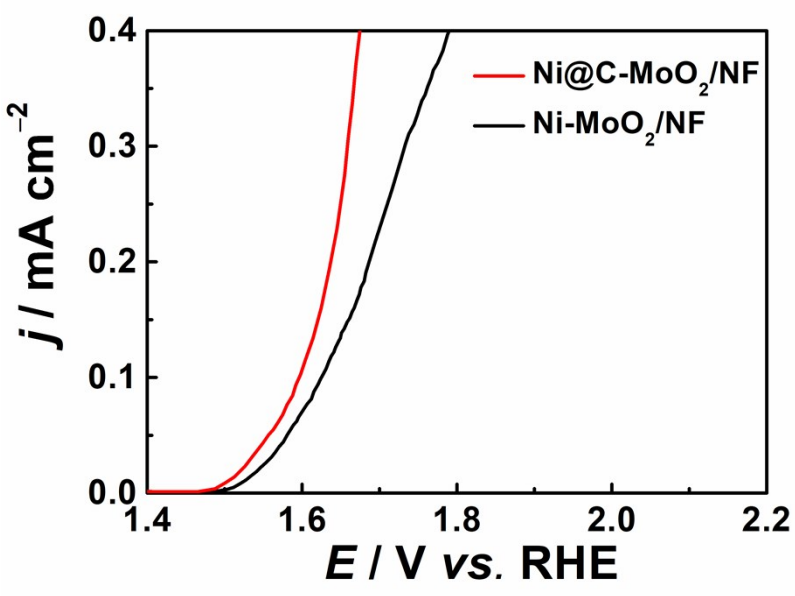

Fig. S19. OER activitiy (current density) of the samples normalized by their ECSAs.

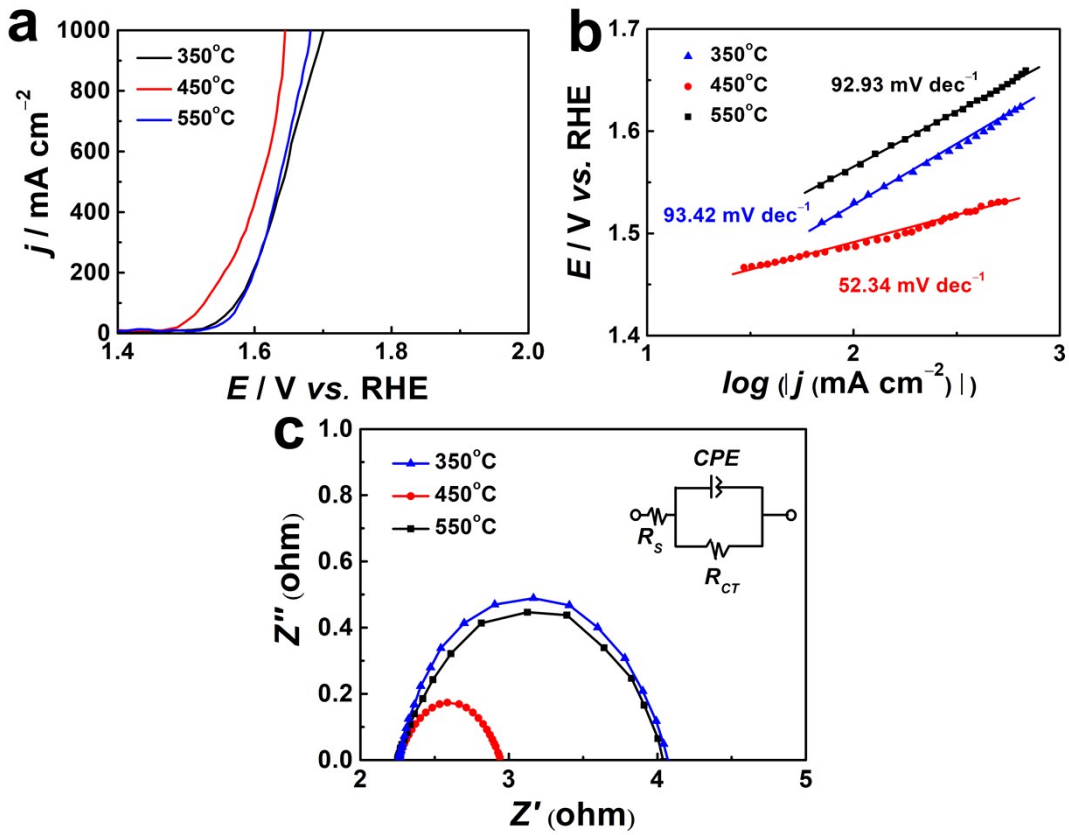

Fig. S20. (a) LSV curves of OER for Ni@C-MoO_2/NF at different temperatures; (b) Corresponding Tafel slopes; (c) Corresponding Nyquist plots tested at 1.60 V for OER with a frequency from 100 kHz to 100 mHz in 1.0 M KOH; Inset is the equivalent circuit model.

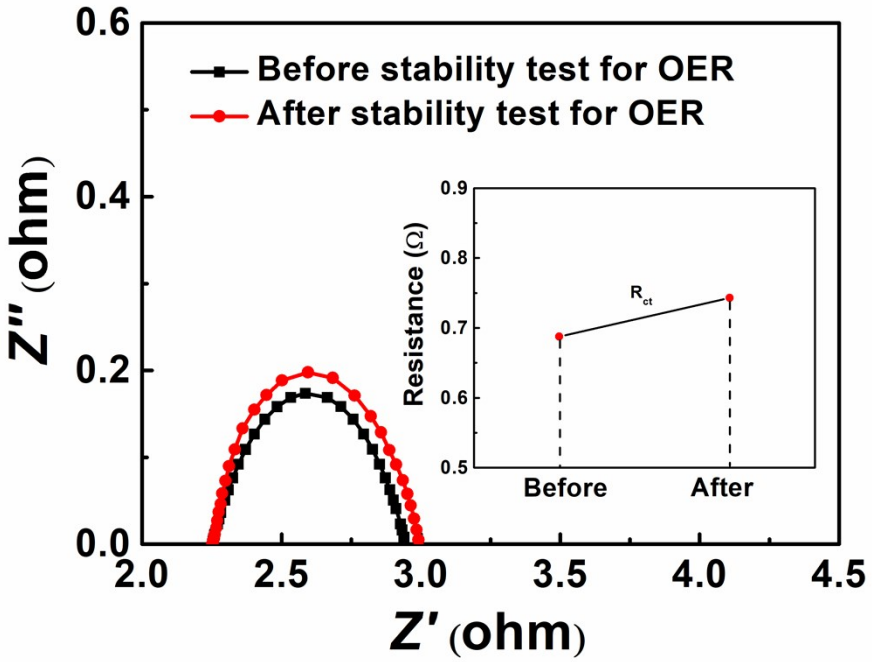

Fig. S21. R_{ct} of Ni@C-MoO_2/NF before and after oxygen evolution stability tests by chronopotentiometry method.

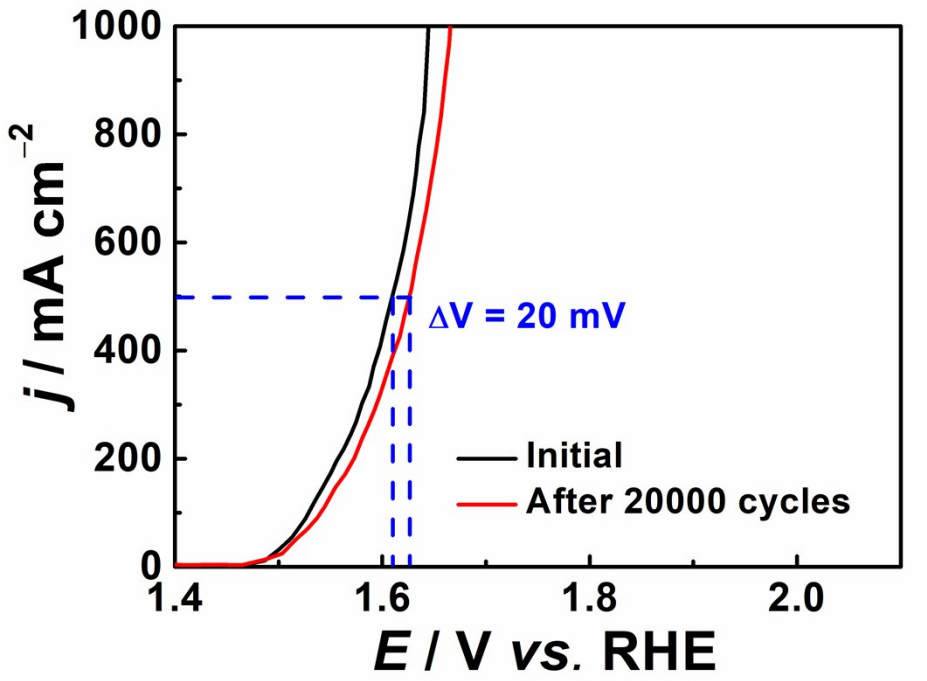

Fig. S22. LSV curves of Ni@C-MoO_2/NF for OER initially and after 20,000 CV cycles, between 1.4 V and 2.0 V.

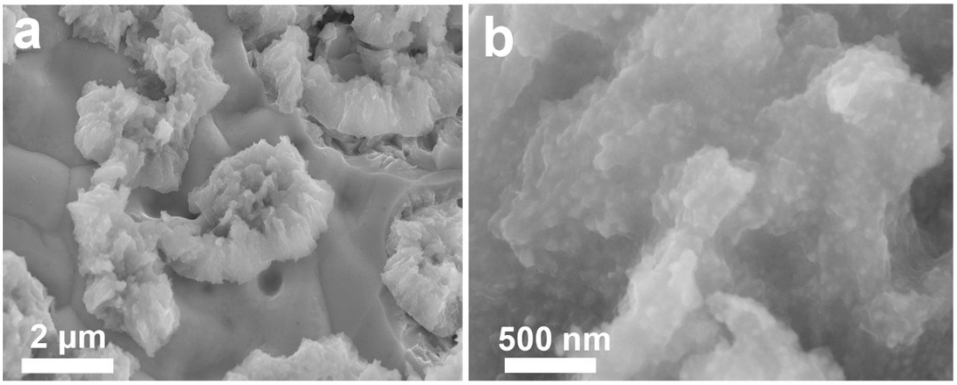

Fig. S23. SEM images of Ni@C-MoO_2/NF after oxygen evolution stability test.

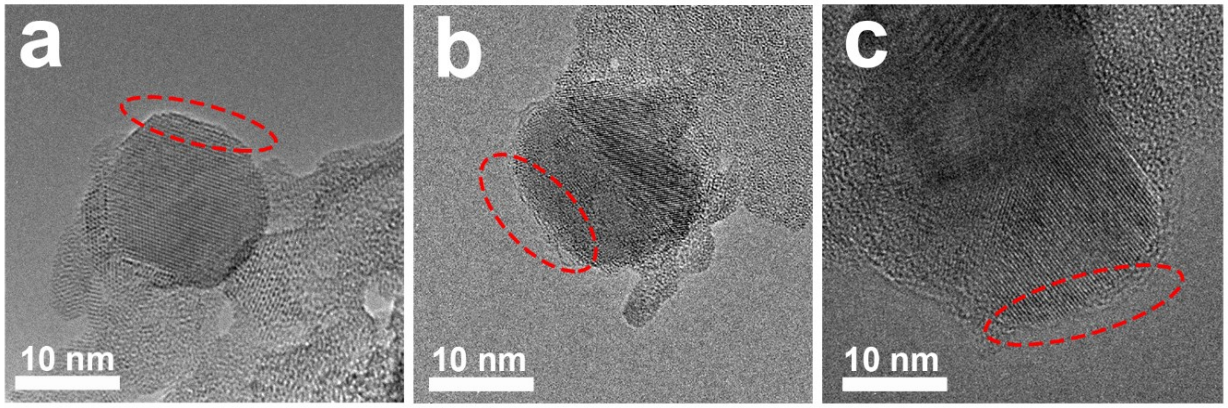

Fig. S24. HRTEM images of Ni@C-MoO_2/NF after oxygen evolution stability test.

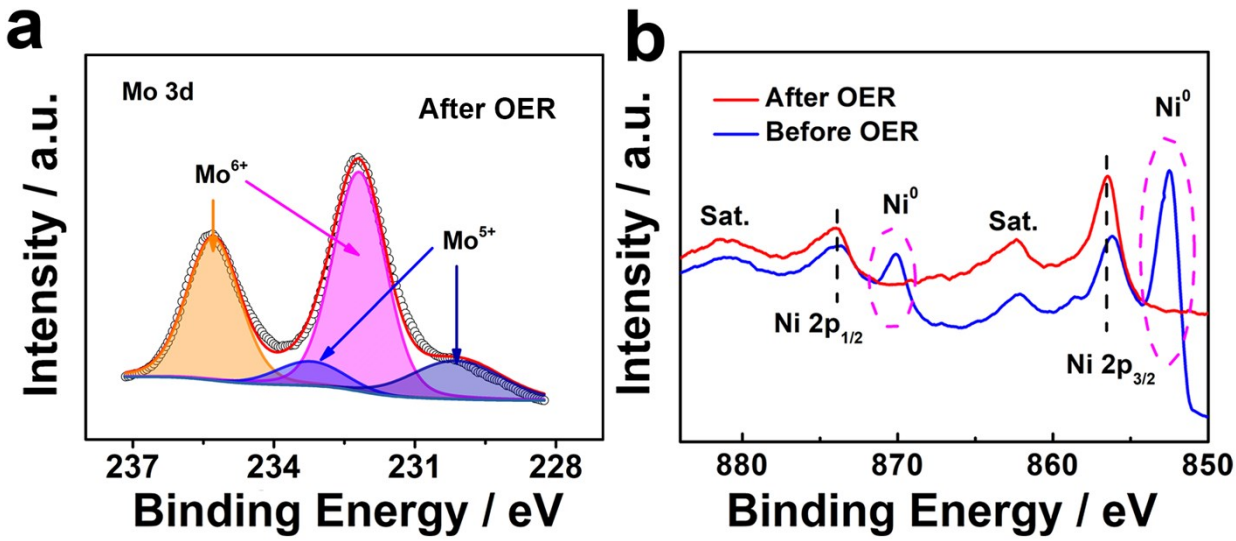

Fig. S25. XPS images of Ni@C-MoO_2/NF for Ni 2p and Mo 3d after oxygen evolution stability test.

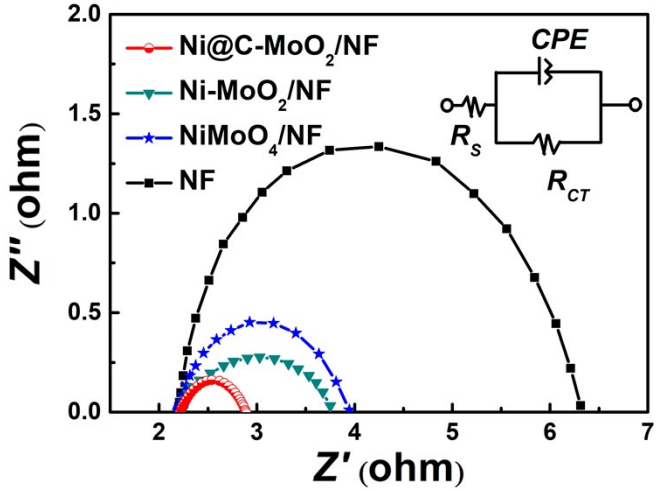

Fig. S26. Nyquist plots tested at 1.60 V for OER with a frequency from 100 kHz to 100 mHz in 1.0 M KOH; Inset is the equivalent circuit model.

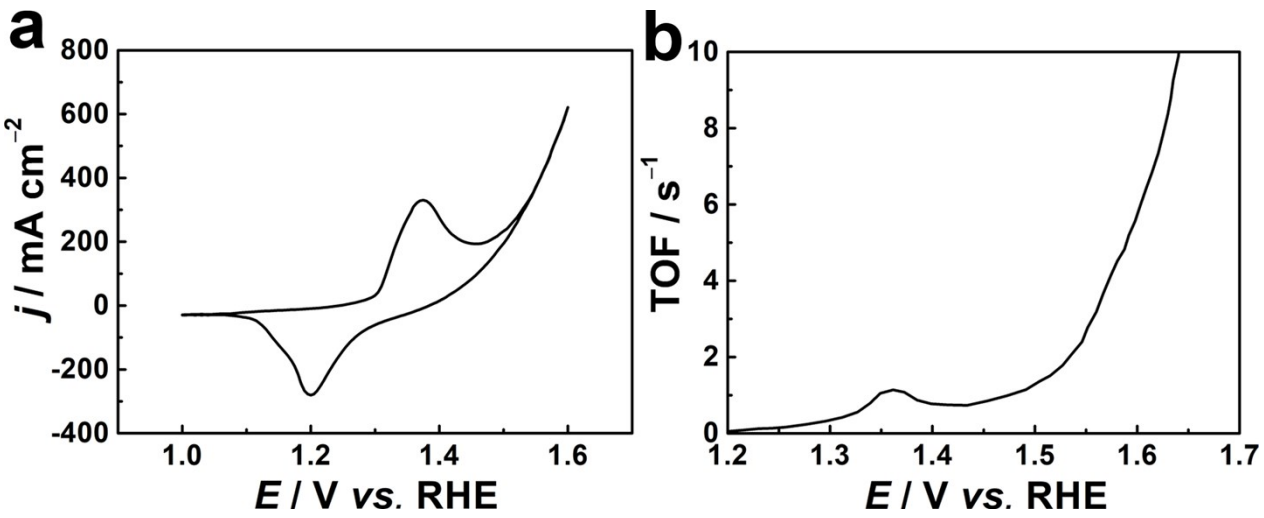

Fig. S27. (a) CV curve of Ni@C-MoO_2/NF for determining the redox surface sites of Ni^{2+}/Ni^{3+} in 1.0 M KOH with a scan rate of 50 mV s^{-1}; (b) The calculated TOFs curve of Ni@C-MoO_2/NF for OER.

We use the active surface redox sites method to study the TOFs of Ni@C-MoO_2/NF for OER, by calculating the redox surface sites of Ni^{2+}/Ni^{3+} without the capacitive current.[9, 10] As shown in Fig. S27a, the Ni@C-MoO_2/NF is tested in 1.0 M KOH solution and the region is 1.0 to 1.6 V vs. RHE. The total number of active atoms is equal to the calculated charge of the peak Q_s divided by the charge of an electron (1.6×10^{-19} C), $N_s = Q_s/Q_e$, which is from the one electron reaction of

Ni^{2+}/Ni^{3+}.[5] In Fig. S27b, the polarization curve is normalized by the active sites and expressed in terms of TOFs, and the TOFs at 1.53V is 1.9 s^{-1} in alkaline media, which is higher than previous reports.[11-13] The high TOFs value of OER could be ascribed to the ultra-thin N-doped-graphene encapsulated Ni structure, which can boost the intrinsic activity of active sites to improve the catalytic activity for OER.[14-16]

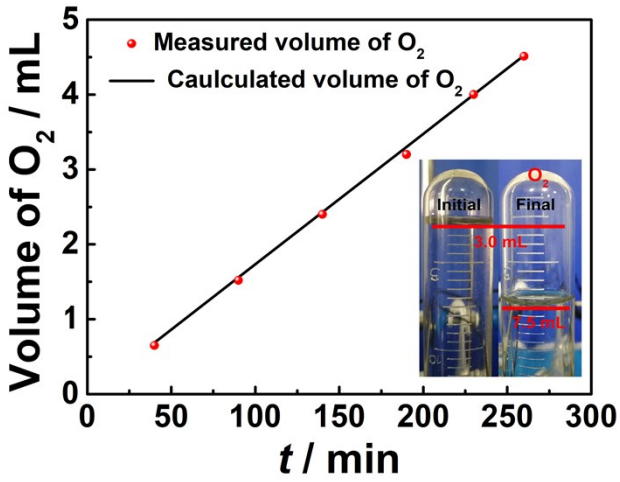

Fig. S28. Amount of hydrogen theoretically calculated and experimentally measured at the current of 5.0 mA versus time for Ni@C-MoO_2/NF in 1.0 M KOH aqueous solution. Inset: the photo indicates that the volume of oxygen after 260 minutes is 4.5 ml.

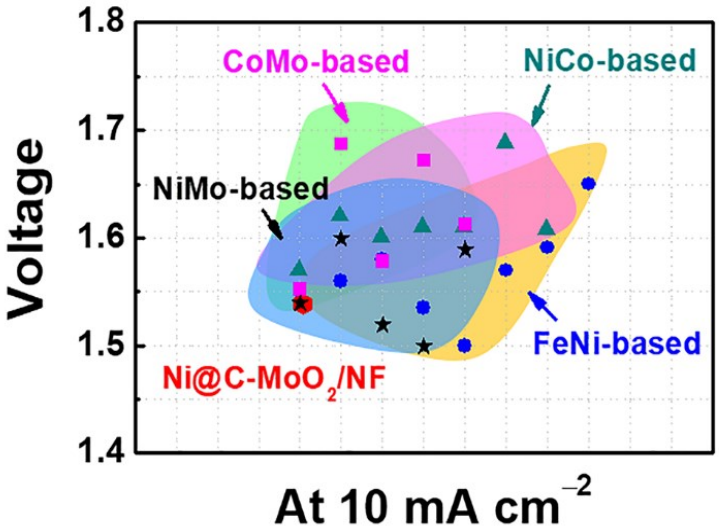

Fig. S29. Activity comparisons of references for water splitting. The overpotential (η_{10}) and voltage at a current density of 10 mA cm^{-2}.

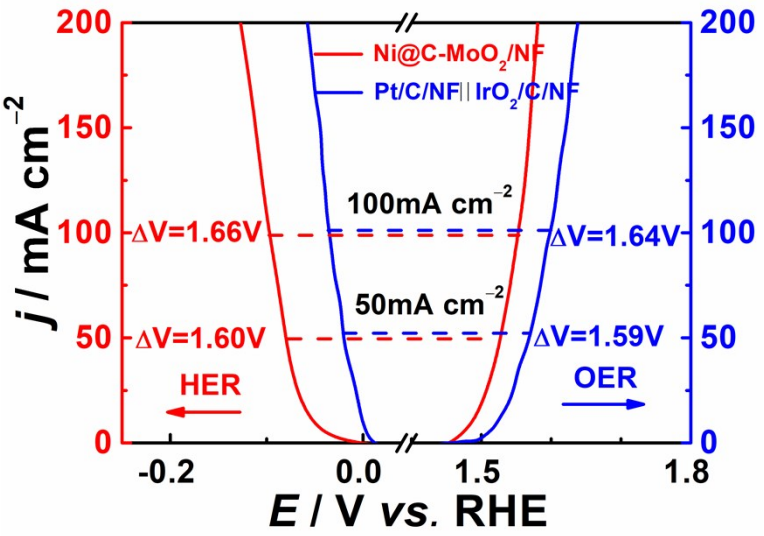

Fig. S30. Steady-state polarization curves of Ni@C-MoO_2/NF, 40 wt.% IrO_2/C/NF and 20 wt.% Pt/C/NF in 1.0 M KOH for HER and OER.

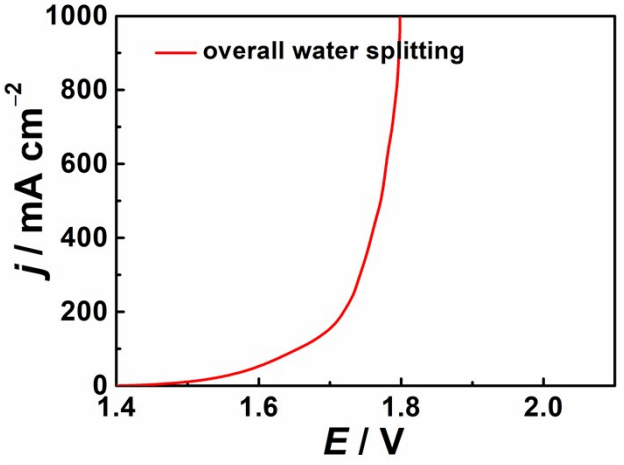

Fig. S31. The LSV curve of Ni@C MoO_2/NF as electrodes for overall water splitting.

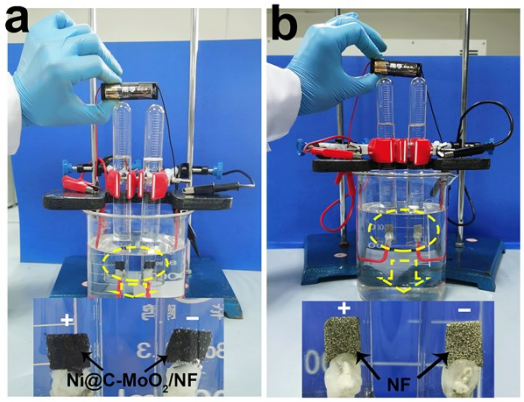

Fig. S32. The pictures of (a) Ni@CMoO_2/NF and (b) NF as electrodes drove by a 1.5 V battery for overall water splitting.

3. Supplementary tables

Table S1. The BET results of Ni@C-MoO_2/NF and $NiMoO_4$/NF.

Catalysts	BET surface areas (m^2/g)	Pore volume($cm^3\ g^{-1}$)	Pore size(nm)
Ni@C-MoO_2/NF	41.5597	0.031	17.4
$NiMoO_4$/NF	7.3510	0.2367	22.8

Table S2. The vales of Ni 2p for differetent samples.

Catalysts	Ni^{2+} $2p_{1/2}$ (eV)	Ni^{2+} $2p_{3/2}$ (eV)	Ni^0 $2p_{1/2}$ (eV)	Ni^0 $2p_{3/2}$ (eV)
Ni@C-MoO_2/NF	873.9	856.1	870.1	852.3
Ni-MoO_2/NF	873.5	855.7	869.7	851.9

Table S3. Comparisons of HER activity of Ni@C-MoO_2/NF with other reported non-noble-metal catalysts.

Catalysts	η_{10} (mV)	η_{100} (mV)	η_{500} (mV)	Tafel slop (mV dec^{-1})	References
Ni@C-MoO_2/NF	25	90	197	44.23	This work
NFN-MOF/NF	87	–	293	35.2	17
$Ni_{2(1-x)}Mo_{2x}P$	72	162	240	46.6	18
CoP(MoP)-$CoMoO_3$@CN	198	–	–	72	19
$MoS_2/Fe_5Ni_4S_8$	120	–	–	45.1	20
N-$NiMoO_4/NiS_2$	99	281	–	74.2	21
$Ni_{0.9}Fe_{0.1}$/NC	111	–	–	231	22
Co-Ni_3N	194	–	–	156	23
N-CNTs/NiS_2@Mo_2C	227	–	–	114.6	24
MoS_2-Ni_3S_2	98	191	–	61	25
NiFe-NC	197	–	–	130	26
Cr-doped FeNi–P/NCN	190	–	–	68.51	6
NiFe LDH@NiCoP/NF	120	–	–	88.2	27
$Ni_{0.75}Fe_{0.125}V_{0.125}$-LDHs/NF	125	–	–	39.4	28
S-$NiFe_2O_4$/NF	138	–	–	61.3	29
MoS_2/NiS_2-3	62	131		50.1	30
Co-NC@Mo_2C	99	–	–	65	31
Co-Mo_2N hybrid	76	–	–	61	32
Co_9S_8@MoS_2	143	–	–	117	33
Ni-Co-P HNBs	107	–	–	46	34
100-NCT-$NiCo_2S_4$	183	–	–	89.8	35
CoMoV LDH/NF	150	–	–	182	36
$NiCo_2S_4$	148	–	–	119	37
Ni_3S_2@$Co(OH)_2$	110	–	–	63	38

NCAs	156	−	−	82.7	39
$NiCo_2O_4$@C	109	−	−	50.3	40

Table S4. The ΔE_{H^*} and ΔG_{H^*} values of the H^* adsorbed on the surface of different models.

Model	Adsorption site	ΔE_{H^*}/eV	ΔG_{H^*}/eV
Ni(111)@NC	T_N	1.163	1.536
	o-T_C	−0.370	−0.001
	m-T_C	0.413	0.769
	p-T_C	−0.279	0.085
Ni(111)		−0.625	−0.390
NC		0.248	0.615

Table S5. Comparisons of OER activity of Ni@C-MoO_2/NF with other reported non-noble-metal catalysts.

Catalysts	η_{10} (mV)	η_{100} (mV)	η_{500} (mV)	Tafel slop (mV dec^{-1})	References
Ni@C-MoO_2/NF	240	290	360	52.34	This work
NFN-MOF/NF	240	–	360	58.8	17
$Ni_{2(1-x)}Mo_{2x}P$	–	340	–	–	18
CoP(MoP)-$CoMoO_3$@CN	296	–	–	105	19
MoS_2/$Fe_5Ni_4S_8$	206	–	–	28.6	20
N-$NiMoO_4$/NiS_2	283	335	–	44.3	21
$Ni_{0.9}Fe_{0.1}$/NC	330	–	–	45	22
Co-Ni_3N	307	–	–	57	23
N-CNTs/NiS_2@Mo_2C	320	–	–	77.5	24
MoS_2-Ni_3S_2	249	340	–	57	25
NiFe-NC	250	–	–	48	26
Cr-doped FeNi-P/NCN	240	–	–	72.36	6
NiFe LDH@NiCoP/NF	220	–	–	48.6	27
$Ni_{0.75}Fe_{0.125}V_{0.125}$-LDHs/NF	231	–	–	62	28
S-$NiFe_2O_4$/NF	267	–	–	36.7	29
MoS_2/NiS_2-3	278	393		91.7	30
Co-NC@Mo_2C	347	–	–	61	31
Co-Mo_2N hybrid	296	–	–	93	32
Co_9S_8@MoS_2	340	–	–	94	33
Ni-Co-P HNBs	270	–	–	76	34
100-NCT-$NiCo_2S_4$	280	–	–	86.8	35
CoMoV LDH/NF	270	–	–	106	36
$NiCo_2S_4$	249	–	–	95	37
Ni_3S_2@$Co(OH)_2$	257	–	–	63.1	38
NCAs	320	–	–	69.4	39
$NiCo_2O_4$@C	270	–	–	46.5	40

Table S6. Comparisons of the overall water splitting activity of the combination of Ni@C-MoO_2/NF with other reported non-noble-metal catalysts.

Catalysts	Voltage at 10 mA cm^{-2} (V)	References
Ni@C-MoO_2/NF	1.54	This work
NFN-MOF/NF	1.56	17
CoP(MoP)-$CoMoO_3$@CN	1.55	19
N-$NiMoO_4$/NiS_2	1.60	21
$Ni_{0.9}Fe_{0.1}$/NC	1.58	22
N-CNTs/NiS_2@Mo_2C	1.52	24
MoS_2-Ni_3S_2	1.50	25
Cr-doped FeNi-P/NCN	1.50	6
NiFe LDH@NiCoP/NF	1.57	27
$Ni_{0.75}Fe_{0.125}V_{0.125}$-LDHs/NF	1.591	28
S-$NiFe_2O_4$/NF	1.65	29
MoS_2/NiS_2-3	1.59	30
Co-NC@Mo_2C	1.685	31
Co-Mo_2N hybrid	1.576	32
Co_9S_8@MoS_2	1.67	33
Ni-Co-P HNBs	1.62	34
100-NCT-$NiCo_2S_4$	1.60	35
CoMoV LDH/NF	1.61	36
$NiCo_2S_4$	1.61	37
Ni_3S_2@$Co(OH)_2$	1.61	38
NCAs	1.688	39
$NiCo_2O_4$@C	1.608	40

4. Supplementary references

1 J. K. Nørskov, T. Bligaard, A. Logadottir, J. R. Kitchin, J. G. Chen, S. Pandelov and J. K. Norskov, *J. Electrochem. Soc.*, 2005, **152**, J23-J26.

2 D. Merki, S. Fierro, H. Vrubel and X. L. Hu, *Chem. Sci.*, 2011, **2**, 1262-1267.

3 E. J. Popczun, J. R. McKone, C. G. Read, A. J. Biacchi, A. M. Wiltrout, N. S. Lewis and R. E. Schaak, *J. Am. Chem. Soc.*, 2013, **135**, 9267-9270.

4 H. J. Yan, Y. Xie, Y. Q. Jiao, A. P. Wu, C. G. Tian, X. M. Zhang, L. Wang and H. G. Fu, *Adv. Mater.*, 2018, **30**, 1704156.

5 H. J. Yan, Y. Xie, A. P. Wu, Z. C. Cai, L. Wang, C. G. Tian, X. M. Zhang and H. G. Fu, *Adv. Mater.*, 2019, **31**, 1901174.

6 Y. Q. Wu, X. Tao, Y. Qing, H. Xu, F. Yang, S. Luo, C. H. Tian, M. Liu and X. H. Lu, *Adv. Mater.*, 2019, **31**, 1900178.

7 S. Y. Jing, J. J. Lu, G. T. Yu, S. B. Yin, L. Luo, Z. S. Zhang, Y. F. Ma, W. Chen and P. K. Shen, *Adv. Mater.*, 2018, **30**, 1705979.

8 J. Yang, D. H. Guo, S. L. Zhao, Y. Lin, R. Yang, D. D. Xu, N. E. Shi, X. S. Zhang, L. Z. Lu, Y. Q. Lan, J. C. Bao and M. Han, *Small*, 2019, **15**, 1804546.

9 X. X. Zou, A. Goswami and T. Asefa, *J. Am. Chem. Soc.*, 2013, **135**, 17242-17245.

10 Y. Z. Xue, Z. Y. Ren, Y. Xie, S. C. Du, J. Wu, H. Y. Meng and H. G. Fu, *Nanoscale*, 2017, **9**, 16256-16263.

11 X. X. Guo, R. M. Kong, X. P. Zhang, H. T. Du and F. L. Qu, *ACS Catal.*, 2017, **8**, 651-655.

12 S. Nandi, S. K. Singh, D. Mullangi, R. Illathvalappil, L. George, C. P. Vinod, S. Kurungot and R. Vaidhyanathan, *Adv. Energy Mater.*, 2016, **6**, 1601189.

13 X. M. Zhou, X. T. Shen, Z. M. Xia, Z. Y. Zhang, J. Li, Y. Y. Ma and Y. Q. Qu, *ACS Appl. Mater. Interfaces*, 2015, **7**, 20322-20331.

14 Y. C. Tu, P. J. Ren, D. H. Deng and X. H. Bao, *Nano Energy*, 2018, **52**, 494-500.

15 L. Pei, J. S. Zhong, T. Z. Li, W. F. Bai, S. T. Wu, Y. J. Yuan, Y. F. Chen, Z. T. Yu, S. C. Yan and Z. G. Zou, *J. Mater. Chem. A*, 2020, **8**, 6795-6803.

16 X. J. Cui, P. J. Ren, C. Ma, J. Zhao, R. X. Chen, S. M. Chen, N. P. Rajan, H. B. Li, L. Yu, Z. Q. Tian and D. H. Deng, *Adv. Mater.*, 2020, 1908126.

17 D. S. Raja, X. F. Chuah and S. Y. Lu, *Adv. Energy Mater.*, 2018, **8**, 1801065.

18 L. Yu, I. K. Mishra, Y. L. Xie, H. Q. Zhou, J. Y. Sun, J. Q. Zhou, Y. Z. Ni, D. Luo, F. Yu, Y. Yu, S. Chen and Z. F. Ren, *Nano Energy*, 2018, **53**, 492-500.

19 L. Yu, Y. Xiao, C. L. Luan, J. T. Yang, H. Y. Lbw, Y. Wang, X. Zhang, X. P. Dai, Y. Yang and H. H. Zhao, *ACS Appl. Mater. Interfaces*, 2019, **11**, 6890-6899.

20 Y. Wu, F. Li, W. L. Chen, Q. Xiang, Y. L. Ma, H. Zhu, P. Tao, C. Y. Song, W. Shang, T. Deng and J. B. Wu, *Adv. Mater.*, 2018, **30**, 1803151.

21 L. An, J. R. Feng, Y. Zhang, R. Wang, H. W. Liu, G. C. Wang, F. Y. Cheng and P. X. Xi, *Adv. Funct. Mater.*, 2019, **29**, 1805298.

22 X. Zhang, H. M. Xu, X. X. Li, Y. Y. Li, T. B. Yang and Y. Y. Liang, *ACS Catal.*, 2015, **6**, 580-588.

23 C. R. Zhu, A. L. Wang, W. Xiao, D. L. Chao, X. Zhang, N. H. Tiep, S. Chen, J. N. Kang, X. Wang, J. Ding, J. Wang, H. Zhang and H. J. Fan, *Adv. Mater.*, 2018, **30**, 1705516.

24 J. Y. Wang, T. Ouyang, Y. P. Deng, Y. S. Hong and Z. Q. Liu, *J. Power Sources*, 2019, **420**, 108-117.

25 Y. Q. Yang, K. Zhang, H. L. Lin, X. Li, H. C. Chan, L. C. Yang and Q. S. Gao, *ACS Catal.*, 2017, **7**, 2357-2366.

26 A. Kumar and S. Bhattacharyya, *ACS Appl. Mater. Interfaces*, 2017, **9**, 41906-41915.

27 H. J. Zhang, X. P. Li, A. Hahnel, V. Naumann, C. Lin, S. Azimi, S. L. Schweizer, A. W. Maijenburg and R. B. Wehrspohn, *Adv. Funct. Mater.*, 2018, **28**, 1706847.

28 K. N. Dinh, P. L. Zheng, Z. F. Dai, Y. Zhang, R. Dangol, Y. Zheng, B. Li, Y. Zong and Q. Y. Yan, *Small*, 2018, **14**, 1703257.

29 J. L. Liu, D. D. Zhu, T. Ling, A. Vasileff and S. Z. Qiao, *Nano Energy*, 2017, **40**, 264-273.

30 J. H. Lin, P. C. Wang, H. H. Wang, C. Li, X. Q. Si, J. L. Qi, J. Cao, Z. X. Zhong, W. D. Fei and J. C. Feng, *Adv. Sci.*, 2019, **6**, 1900246.

31 Q. R. Liang, H. H. Jin, Z. Wang, Y. L. Xiong, S. Xiong, X. C. Zeng, D. P. He and S. C. Mu, *Nano Energy*, 2019, **57**, 746-752.

32 X. Shi, A. P. Wu, H. J. Yan, L. Zhang, C. G. Tian, L. Wang and H. G. Fu, *J. Mater. Chem. A*, 2018, **6**, 20100-20109.

33 J. Bai, T. M. Meng, D. L. Guo, S. G. Wang, B. G. Mao and M. H. Cao, *ACS Appl. Mater. Interfaces*, 2018, **10**, 1678-1689.

34 E. L. Hu, Y. F. Feng, J. W. Nai, D. Zhao, Y. Hu and X. W. Lou, *Energy Environ. Sci.*, 2018, **11**, 872-880.

35 F. Li, R. C. Xu, Y. M. Li, F. Liang, D. F. Zhang, W. F. Fu and X. J. Lv, *Carbon*, 2019, **145**, 521-528.

36 J. Bao, Z. L. Wang, J. F. Xie, L. Xu, F. C. Lei, M. L. Guan, Y. Zhao, Y. P. Huang and H. M. Li, *Chem. Commun.*, 2019, **55**, 3521-3524

37 C. Zequine, S. Bhoyate, K. Siam, P. K. Kahol, N. Kostoglou, C. Mitterer, S. J. Hinder, M. A. Baker, G. Constantinides, C. Rebholz, G. Gupta, X. L. Li and R. K. Gupta, *Surf. Coat. Technol.*, 2018, **354**, 306-312.

38 S. P. Wang, L. Xu and W. X. Lu, *Appl. Surf. Sci.*, 2018, **457**, 156-163.

39 B. Zhang, X. M. Zhang, Y. Wei, L. Xia, C. R. Pi, H. Song, Y. Zheng, B. Gao, J. J. Fu and P. K. Chu, *J. Alloys Compd.*, 2019, **797**, 1216-1223.

40 J. Deng, H. J. Zhang, Y. Zhang, P. Luo, L. Liu and Y. Wang, *J. Power Sources*, 2017, **372**, 46-53.